Giant diffusion of underdamped particles in a biased periodic potential

Benjamin Lindner[1,2] and Igor M. Sokolov[1]
[1]*Department of Physics, Humboldt Universität zu Berlin, Newtonstr 15, 12489 Berlin, Germany*
[2]*Bernstein Center for Computational Neuroscience, Haus 2, Philippstr 13, 10115 Berlin, Germany*
(Received 23 February 2016; published 6 April 2016)

We consider the diffusive properties of Brownian motion in a biased periodic potential. We relate the effective diffusion coefficient to the solution of two coupled time-independent partial differential equations and solve these equations numerically by the matrix-continued-fraction (MCF) method for intermediate values of the temperature and friction coefficient. The weak-noise limit is explored by numerical simulations of the Langevin equations. Here, we identify the regions of parameters for which the diffusion coefficient exponentially grows with inverse temperature. In particular, we demonstrate that there is a finite range of bias forces for which such a growth is observed (region of giant enhancement of diffusion). We also show that at small forces close to the critical range, the diffusion coefficient possesses a pronounced maximum as a function of temperature. All results can be interpreted in the framework of a simple two-state theory incorporating the transition rates between the locked and running solutions.

DOI: 10.1103/PhysRevE.93.042106

I. INTRODUCTION

The dynamics of Brownian particles in an inclined cosine potential is a basic nonequilibrium model of statistical physics that describes a surprising range of systems, including the damped pendulum with torque [1], Josephson junctions [2], superionic conduction [3], and the dynamics of phase-locked loops [4]. The problem is attractive because it is simple to formulate; it has many applications but also possesses a rich phenomenology as a nonlinear stochastic system.

Brownian particles in a biased cosine potential

$$U(x) = -Fx - d\cos(x) \tag{1}$$

(with bias force F) obey the following equations of motion

$$\dot{x} = v, \quad \dot{v} = -\gamma v - U'(x) + \sqrt{2\gamma kT}\xi(t). \tag{2}$$

Here γ is the Stokes friction coefficient, kT is the thermal energy, and $\xi(t)$ is Gaussian white noise with intensity 1. We consider particles with unit mass $m = 1$ and a potential with unit amplitude (prefactor of the cosine part is 1), which amounts to renormalization of time and space units [1].

The long-term (asymptotic) properties of Brownian particles are characterized by their mean velocity

$$\langle v\rangle = \lim_{t\to\infty} \frac{\langle x(t) - x(0)\rangle}{t} \tag{3}$$

and the diffusional spreading around this mean motion, quantified by an effective diffusion coefficient

$$D_{\rm eff} = \lim_{t\to\infty} \frac{\langle [x(t) - \langle x(t)\rangle]^2\rangle}{2t}. \tag{4}$$

The mean velocity has been explored in much detail in the seminal work by Risken *et al.* [5,6] and is exhaustively discussed in Risken's well-known textbook [1]. The diffusion coefficient, in particular with finite bias force, has turned out to be a much more difficult subject [3,7–10] and remains a vibrant topic of current research both in theory [11–15] and experiment [16–19]. Already in the comparatively simple overdamped limit ($\gamma \gg 1$), for instance, the diffusion coefficient is enhanced and exceeds the bare diffusion coefficient of free diffusion $D_0 = kT/\gamma$ by orders of magnitude if the force is close to a critical value [9]. This enhancement of diffusion becomes particularly pronounced for low temperatures and implies that the diffusion coefficient will diverge for $T \to 0$ if we poise the bias force exactly at its critical value.

In numerical studies, even stronger amplification of diffusion has been observed in the underdamped case [8,11] due to a bistability of the velocity dynamics. The latter phenomenon is well known since the work by Risken and coworkers [1,5,6], who found that at low friction the velocity can be locally stable in a locked solution (the particle is captured in a local potential minimum) but also in a running solution [the particle gains enough energy to overcome dissipative losses, see Fig. 1(a) for an illustration]. To observe bistability, the constant force should be in a range

$$F_1(\gamma) < F < F_3 = 1, \tag{5}$$

which can be found from solutions of the deterministic system; this range is indicated as the shaded area in Fig. 2. With noise, the dynamics is marked by stochastic transitions between locked and running states [Fig. 1(b)]. These two states become equally likely for $T \to 0$ on a line $F_2(\gamma)$ (dashed line in Fig. 2), which can be found as the force at which the mean velocity jumps from zero to a finite value in the limit of vanishing temperature [1]. Our result for $F_2(\gamma)$ is obtained numerically and differs for γ close to unity from the result by Ref. [6]. The latter result was based on the matrix-continued-fraction approach, which breaks down at low temperatures.

Returning to the diffusion problem, in Ref. [11] it has been suggested that the maximal diffusion coefficient grows with inverse temperature like a power law and that the force range of diffusion enhancement shrinks to zero when approaching zero temperature. The first claim has been recently disputed in Ref. [14], where it was shown that the growth of the maximal diffusion coefficient follows an exponential dependence on the inverse noise intensity (temperature). This is consistent with another example of noise-driven bistable velocity dynamics, the one-dimensional active Brownian motion [20,21].

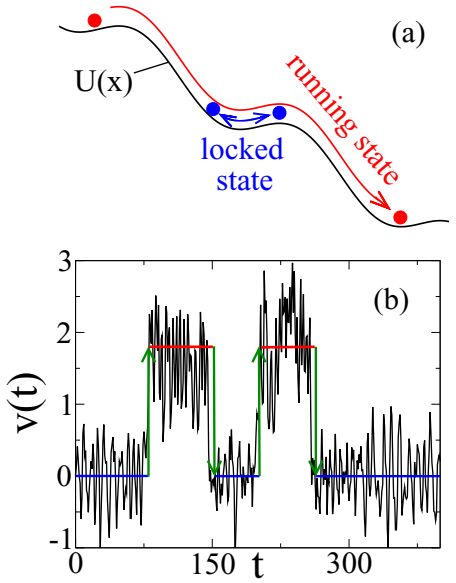

FIG. 1. Underdamped particles in the inclined potential show a bistable velocity dynamics. Underdamped Brownian motion in a biased periodic potential as shown in (a) switches between a running state (red particle), in which the gain from potential energy balances the dissipative losses and a locked state (blue particle), in which the particle oscillates stochastically around the potential minimum. In the velocity, transitions (green arrows) between the states (red and blue) can be easily identified (b). Parameters: $\gamma = 0.4, F = 0.721$.

Our study contributes a number of results to the diffusion problem in the underdamped case. First, we derive an expression for the diffusion coefficient in terms of the solution of two coupled time-independent partial differential equations and explain in the Appendix how these equations can be solved by the matrix-continued-fractions techniques. Second, we use extensive numerical simulations to determine for all values of the friction coefficient the range of forces in which the diffusion coefficient diverges in the zero-temperature limit.

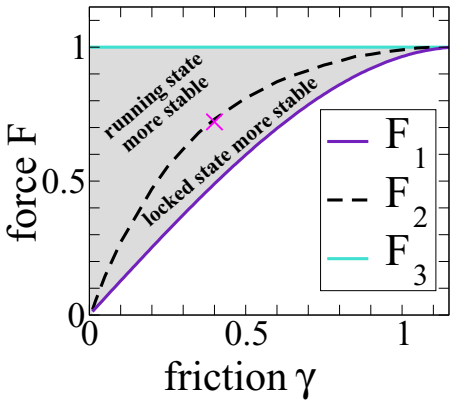

FIG. 2. Range of bistability of the model (Risken plot). Bistability is only observed if force and friction are within a particular parameter region (gray area), which is further subdivided into regions above and below $F_2(\gamma)$ [dashed line in (a)], in which the running or the locked state is more stable, respectively, in the zero-temperature limit. Parameters used in Fig. 1 are indicated by the magenta cross.

We show in particular that in the underdamped case, the range of forces for which diffusion is enhanced does not vanish. Third, we underpin our numerical findings with a simple two-state theory, previously developed for an active Brownian motion model with bistable velocity dynamics [21] and applied in the current context to the problem of maximal diffusion in Ref. [14]. In addition, this theory predicts that for certain forces the diffusion coefficient should display a strong maximum upon variation of temperature, a finding that we confirm numerically.

II. DIFFUSION COEFFICIENT DETERMINED FROM THE FOKKER-PLANCK EQUATION

As outlined in the following, we can determine mean velocity and diffusion coefficient from the Fokker-Planck equation for the probability density $P(x,v,t)$ corresponding to the Langevin Eq. (2):

$$\partial_t P = \hat{L}_{\rm FP} P, \tag{6}$$

which is defined in terms of the operator

$$\hat{L}_{\rm FP}(x,v) = -v\partial_x + \partial_v(\gamma v + d\sin x - F + \gamma kT\partial_v). \tag{7}$$

The stationary solution is found from

$$\hat{L}_{\rm FP} P_0(x,v) = 0 \tag{8}$$

and allows to calculate the mean velocity [1]

$$\langle v\rangle = \int_{-\infty}^{\infty} dv \int_{-\infty}^{\infty} dx\ v\ P_0(x,v). \tag{9}$$

The time-dependent solution of the Fokker-Planck equation in the form of an eigenfunction expansion can be used to determine the diffusion coefficient [7]. Here, we pursue an alternative approach that does not require us to solve for the eigenvalues of the Fokker-Planck equation but instead consists of solving two coupled time-independent equations.

In order to connect the effective diffusion coefficient to the solution of Eq. (6), we recall the Kubo relation

$$D_{\rm eff} = \int_0^{\infty} d\tau \langle [v(\tau) - \langle v\rangle][v(0) - \langle v\rangle]\rangle, \tag{10}$$

in which we can express the velocity autocorrelation function by the transition probability density $P(x,v,\tau|x_0,v_0,0)$ as follows:

$$\begin{aligned}\langle v(\tau)v(0)\rangle - \langle v\rangle^2 &= \int dv_0 \int dv \int dx_0 \int dx\ v\ v_0 \\ &\times [P(x,v,\tau|x_0,v_0,0) - P_0(x,v)]P_0(x_0,v_0),\end{aligned} \tag{11}$$

where all integrals run from $-\infty$ to ∞ both in space and velocity variables.

Combining this expression with Eq. (10), we can write

$$D_{\rm eff} = \int dv\ v \int dx\ G(x,v), \tag{12}$$

where

$$\begin{aligned}G(x,v) = \int dx_0 \int dv_0 \int_0^{\infty} d\tau\ v_0 P_0(x_0,v_0) \\ \times [P(x,v,\tau|x_0,v_0,0) - P_0(x,v)].\end{aligned} \tag{13}$$

In order to derive an equation for $G(x,v)$, we multiply the time-dependent FPE, Eq. (6), [governing $P(x,v,\tau|x_0,v_0,0)$] and the stationary FPE, Eq. (8), [governing $P_0(x,v)$] with $v_0 P_0(x_0,v_0)$. Switching left-hand and right-hand sides of the equation and integrating the difference over the full range of x_0, v_0 and over time we obtain

$$\begin{aligned}\hat{L}_{\mathrm{FP}}(x,v)&G(x,v)\\ &= \int dx_0 \int dv_0 \cdot v_0 P_0(x_0,v_0)\\ &\quad\times \int_0^\infty dt\,\partial_t [P(x,v,t|x_0,v_0 0) - P_0(x,v)]\\ &= \int dx_0 \int dv_0 v_0 [P_0(x,v) - \delta(x-x_0)\delta(v-v_0)] P_0(x_0,v_0).\end{aligned} \tag{14}$$

Hence, the equation governing $G(x,v)$ is an inhomogeneous partial differential equation of second order and in two variables:

$$\hat{L}_{\mathrm{FP}}(x,v)G(x,v) = P_0(x,v)(\langle v\rangle - v). \tag{15}$$

Instead of the densities over the entire x axis, it suffices to consider functions (similar to the treatment of Reimann in Ref. [22])

$$p(x,v) = \sum_{k=-\infty}^{+\infty} P_0(x + k\cdot 2\pi, v), \tag{16}$$

$$g(x,v) = \sum_{k=-\infty}^{+\infty} G(x + k\cdot 2\pi, v), \tag{17}$$

which are by definition periodic in x, i.e.,

$$p(0,v) = p(2\pi,v), \quad g(0,v) = g(2\pi,v). \tag{18}$$

Furthermore, $p(x,v)$ is normalized on the interval $x \in [0,2\pi]$ and $v \in (-\infty,\infty)$

$$\int_0^{2\pi} dx \int_{-\infty}^{+\infty} dv\ p(x,v) = 1, \tag{19}$$

whereas the double integral over $g(x,v)$ yields zero by virtue of Eq. (17) and Eq. (13)

$$\int_0^{2\pi} dx \int_{-\infty}^{+\infty} dv\ g(x,v) = 0. \tag{20}$$

For the velocity variable, natural boundary conditions hold true for both functions

$$\lim_{v\to\pm\infty} p(x,v) = 0, \qquad \lim_{v\to\pm\infty} g(x,v) = 0. \tag{21}$$

To sum up, we have to solve

$$\hat{L}_{\mathrm{FP}}(x,v)p(x,v) = 0, \tag{22}$$

$$\hat{L}_{\mathrm{FP}}(x,v)g(x,v) = p(x,v)(\langle v\rangle - v) \tag{23}$$

with periodic boundary conditions, Eq. (18), in x, natural boundary conditions, Eq. (21), in v, and the normalization conditions Eq. (19) and Eq. (20). The mean velocity in the steady state and the diffusion coefficient in the asymptotic limit are then given by

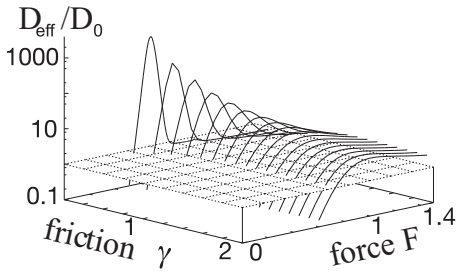

FIG. 3. Diffusion coefficient in the underdamped limit. As a result of the bistable velocity dynamics in the underdamped regime (gray area in the Risken plot in Fig. 2), the diffusion coefficient D_{eff} becomes much larger than the free diffusion coefficient (indicated by the plane) for forces around $F_2(\gamma)$. We show D_{eff} in units of the free coefficient $D_0 = kT/\gamma$ as a function of friction and bias force for $kT = 0.1$ (numerical result by the matrix-continued-fraction method).

$$\langle v\rangle = \int_{-\infty}^{+\infty} dv \int_0^{2\pi} dx\ vp(x,v), \tag{24}$$

$$D_{\mathrm{eff}} = \int_{-\infty}^{+\infty} dv \int_0^{2\pi} dx\ vg(x,v). \tag{25}$$

The equation for $p(x,v)$ and $\langle v\rangle$ has been solved by the matrix-continued-fraction method [1]. The same can be done for the full system for $p(x,v)$ and $g(x,v)$ to determine D_{eff} as outlined in the appendix.

The MCF method works well for moderate to large values of the temperature and allows us to plot D_{eff} as a function of friction coefficient γ and bias force F down to moderate $\gamma \geqslant 0.35$ (Fig. 3). This plot confirms known results from the literature. The enhancement of diffusion, defined by

$$D_{\mathrm{eff}}/D_0 > 1, \tag{26}$$

occurs in the overdamped case [9] around the critical force $F = 1$ at which minima and maxima of the potential merge. A much larger (truly giant) diffusion enhancement is observed for $\gamma < 1.1$ in the underdamped case [8,11]. Here, the maximum diffusion coefficient is attained around the force $F_2(\gamma)$ that is well within the region in which the deterministic velocity dynamics is bistable. We have verified the MCF results by numerical simulations and by the analytical result in the overdamped limit [9,10], which is close to the MCF result already for $\gamma = 2$.

III. LANGEVIN SIMULATION RESULTS FOR SMALL FRICTION AND LOW TEMPERATURE

Of central interest in this work is the behavior of the diffusion coefficient of underdamped particles in the weak-noise limit $T \to 0$. To this end, we have to resort to extensive numerical simulations of the Langevin dynamics Eq. (2). For all combinations of F,γ, and T shown in the following, we simulate 100 particles with a time step of $\Delta t = 0.01$ for a time window of $t_{\max} = 10^5$ (at the smallest noise intensities we ran simulations with $t_{\max} = 10^6$). We ensure that asymptotically the mean-square displacement grows linearly and avoid the range of extremely small $\gamma < 0.01$, in which

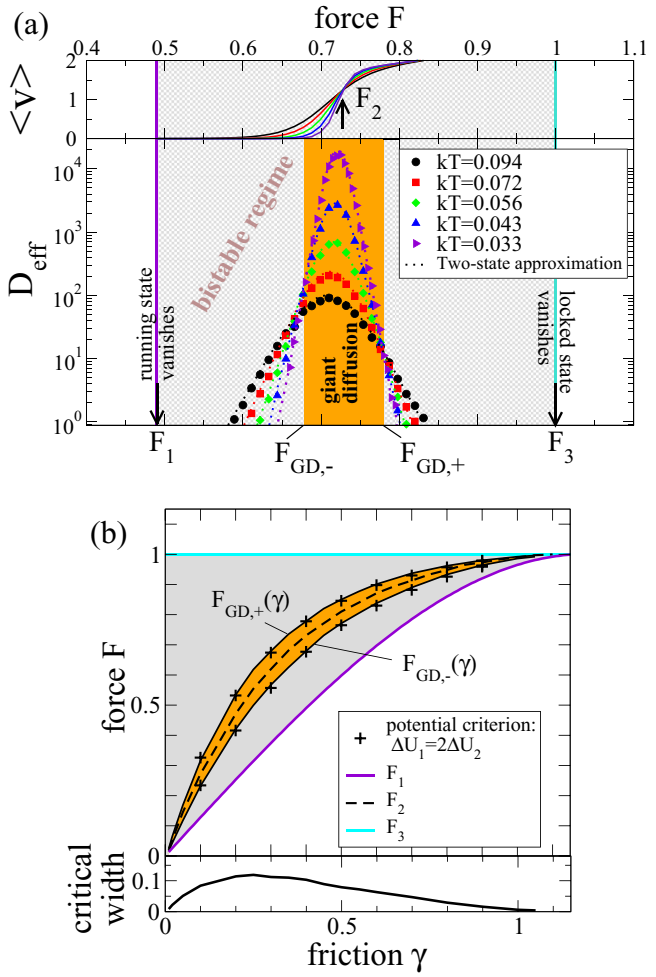

FIG. 4. Finite force range for a giant enhancement of diffusion (a) Mean velocity (top) and diffusion coefficient $D_{\rm eff}$ (bottom) for $\gamma = 0.4$ as a function F for different temperatures as indicated. Three critical values of the force are shown: $F_1 \approx 0.49$ and $F_3 = 1$ in between the velocity dynamics is bistable (gray shaded area), F_2 at which the velocity jumps in the weak noise limit from zero to a finite value (intersection of velocity curves for different temperatures in the top panel). The behavior of the diffusion coefficient for vanishing temperature defines the critical range of bias (orange), corresponding to enhanced diffusion. (b) Risken plot with the three critical forces F_1, F_2, F_3 and the orange band of γ-dependent forces that yield giant enhancement of diffusion. The width of the band passes through a maximum (bottom). Numerical simulation results in (a) and (b) are supported by arguments from a Markovian two-state theory (see text and next figure), that allows for an independent determination of the critical force range [plus signs in (b)] and the diffusion coefficient [dotted lines in (a)].

exceptionally long transients are observed [12]. Besides the diffusion coefficient Eq. (4) we also measure the transition rates from locked to running state and vice versa, respectively.

The results of such simulations for $\gamma = 0.4$ are shown in Fig. 4(a) for varying bias force and different small values of the temperature. The mean velocity (top) displays the well-known sigmoidal behavior and approaches a threshold nonlinearity with decreasing temperature. All velocity curves intersect approximately at the same value of F_2 defined above. Remarkably, the diffusion coefficient (bottom) reveals a strong enhancement in a finite range of the bias force (marked in orange) and attains a pronounced maximum at $F_{\rm max} \approx F_2$. The force values $F_{GD,-}$ and $F_{GD,+}$ that limit the region of enhanced diffusion are well within the region of bistability and can be approximately determined from the intersection points of the diffusion curves $D_{\rm eff}(F)$ for different temperatures (some subtleties regarding these intersection points are discussed below).

We have simulated the system for different values of γ and determined at each value the range of forces with diffusion enhancement. This range corresponds in the (γ, F) plane of Fig. 4(b) to an area marked in orange. The width $F_{GD,+} - F_{GD,-}$ of this area is shown in the bottom panel of Fig. 4(b) and attains a maximum at $\gamma \approx 0.25$. The finite region of diffusion enhancement constitutes the most important result of our study that we will now further support by additional theoretical considerations.

IV. TWO-STATE THEORY OF THE GIANT DIFFUSION IN THE UNDERDAMPED CASE

Within the region of bistability, mean drift and diffusion are shaped mainly by the transitions between locked (L) and running (R) states, which can be represented by a Markovian two-state process in the velocity space. This is a discrete approximation of the velocity dynamics in an effective bistable potential in energy [1] (see also the related heuristic treatment in Ref. [15]).

Given the transition rates $r_{R\to L}$ and $r_{L\to R}$ between the two discrete states, the diffusion coefficient reads [23]

$$D_{\rm eff} = \frac{(F/\gamma)^2 r_{R\to L} r_{L\to R}}{(r_{R\to L} + r_{L\to R})^3}, \tag{27}$$

where we assumed for simplicity that the velocity in the running state is F/γ (slightly overestimating the true velocity [1]), while in the locked state the velocity is zero. Using the transition rates measured in our simulations, we show in Fig. 4(a) the values of the diffusion coefficient according to Eq. (27) by dotted lines. We find an excellent agreement with the corresponding values as obtained in direct simulations. This corroborates the conjecture that the amplification of diffusion in the underdamped case can be fully understood by means of the transition rates for the velocity.

Previous results on both types of transition rates have all the form of an Arrhenius or Kramers law $r \sim \exp[-\Delta U/(kT)]$ but differ in the temperature dependence of the prefactor depending on the exact values of F and γ [5,6,24–26]. From our measurement of the rates for different small temperature values, we can extract effective potential barriers from an Arrhenius plot [see Fig. 5(a)]. Moreover, we also fit a Kramers-like formula with a power-law prefactor (i.e., $r \sim T^\alpha \exp[-\Delta U/(kT)]$) and obtain similar values of the potential barriers. Importantly, we find by this latter procedure that the rate from the running to the locked state is best fit with a power law of $\alpha \approx 0.22$, whereas the transition from the locked to the running state has $\alpha = 0$ (simple Arrhenius dependence). These values are only approximate and hold true for intermediate values of γ and forces around F_2.

The two-state formula for the diffusion coefficient combined with the Kramers-like transition rates predicts that critical values of the force $F_{GD,-}$ and $F_{GD,+}$ are determined

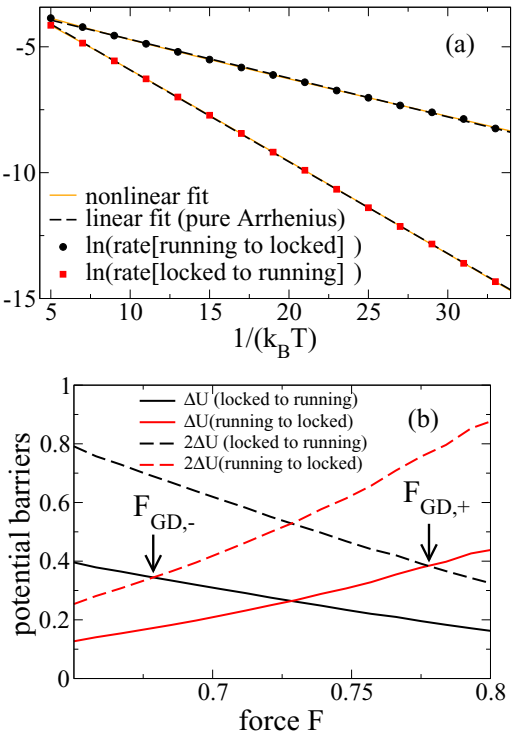

FIG. 5. Extracting effective barriers. The logarithms of the rates plotted as a function of the inverse temperature [Arrhenius plot in (a) for $\gamma = 0.4, F = 0.67$] yield estimates of effective potential barriers (see text). Estimates based on the mean slope (dashed line) or a nonlinear fit that includes a power-law dependence of the prefactor (orange lines) give similar values of the barrier height. Barrier heights are plotted as functions of the force F in (b). Two-state theory based on Kramers rates predicts that critical forces are those for which one potential barrier [solid lines in (b)] equals twice the other barrier [dashed lines in (b)]; the resulting values of the critical forces [indicated by arrows in (b)] are shown in Fig. 4(b) by plus signs.

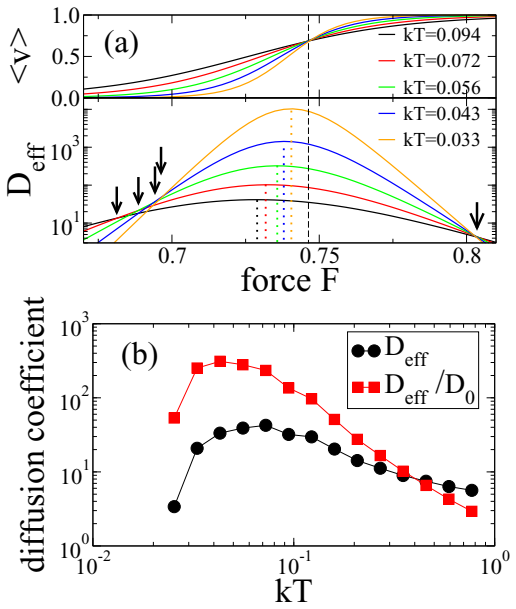

FIG. 6. Finite-temperature effects. Using the two-state theory Eq. (27) with rates $r_{R\to L} = 0.06(kT)^{0.22}\exp[-(2.1F - 1.3)/(kT)]$ and $r_{R\to L} = 0.082\exp[-(1.4 - 1.5F)/(kT)]$, we can reproduce finite-temperature effects on the intersections of diffusion curves [arrows in (a)] and difference between the forces that maximize diffusion [dotted vertical lines in (a)] and that lead to a transition in velocity [dashed vertical line in (a)]. In (b) we show the temperature dependence of D_{eff} for a force F close to but smaller than $F_{GD,-}$. As a consequence of the temperature sensitivity of the left intersection points shown in (a), we observe in this case a pronounced maximum in the diffusion coefficient as a function of temperature [black line in (b)]. This maximum is also present if we plot D_{eff} in units of the free diffusion coefficient D_0 [red line in (b)].

by the condition that one barrier height equals twice the other barrier height [21]. Plotting the values of these heights [solid lines in Fig. 5(b)] and twice these values (dashed lines) as functions of F, we obtain from the two intersection points of solid and dashed lines alternative estimates of $F_{GD,-}$ and $F_{GD,+}$. These are shown for selected values of γ by plus signs in Fig. 4(b). Consistent with the above line of reasoning, the plus signs are close to the border of giant diffusion marked in orange. Moreover, within the range $(F_{GD,-}, F_{GD,+})$ the diffusion coefficient grows exponentially with inverse temperature.

The simple picture we have drawn so far assumed that: (i) all diffusion curves intersect at two points defining $F_{GD,-}$ and $F_{GD,+}$; (ii) the value of force F_2 corresponding to the intersection point of the velocity curves coincides with the force maximizing the diffusion coefficient. A closer inspection of Fig. 4(a) reveals two features that indicate small deviations from this. First, the intersection points of pairs of diffusion curves at the left boundary do not coincide exactly. Second, the intersection of the velocity curves corresponds to a force ($F_2 \approx 0.73$), which is slightly different from the one that maximizes the diffusion coefficient ($F_{\max} \approx 0.72$). Both points should be attained for the force $F_2(\gamma)$ that makes the running and the locked states equally probable. Within the two-state picture, we can understand these small deviations as finite-temperature effects, if we take into account the different values and temperature dependences of the prefactors in the rates.

In Fig. 6 , we plot mean velocity and effective diffusion coefficient of the two-state theory for potential barriers obtained from linear fits of the barriers in Fig. 5(b) and with temperature-dependent prefactors corresponding to the typical values obtained from the nonlinear fit in Fig. 5(a). Clearly, we observe the two effects also present in Fig. 4(a): (i) intersection points of the diffusion curves (indicated by arrows) close to $F_{GD,-}$ fan out whereas those around $F_{GD,+}$ are very close to each other; (ii) forces at which diffusion is maximized (dotted vertical lines) depend on temperature and are generally slightly smaller than the force at which the different velocity curves intersect (dashed vertical line). Summarizing, we can regard these deviations as a consequence of the different temperature dependence of the Kramers rates. It is also worth emphasizing that according to the two-state theory the deviations vanish for $T \to 0$. However, in the continuous system Eq. (2) a much smaller temperature than we have used would require exponentially larger simulation times.

A remarkable consequence of the finite temperature dependence of the diffusion curves is demonstrated in Fig. 6(b) for the original system Eq. (2). Choosing a subcritical force $F = 0.67$, which is close to but smaller than $F_{GD,-}$, we

find a pronounced maximum in the diffusion coefficient as a function of temperature. When we plot this in units of the free diffusion coefficient D_0 (proportional to the temperature), we still obtain a maximum because outside the critical force range, the diffusion coefficient goes exponentially to zero for $T \to 0$.

V. SUMMARY AND CONCLUSIONS

In this paper we have studied the underdamped Brownian motion in an inclined periodic potential, a standard problem of statistical physics of nonequilibrium systems. Based on the Kubo relation, we found a connection between the effective diffusion coefficient and the solution of two coupled time-independent partial differential equations. The derived connection may also provide the basis for analytical approximations for the diffusion coefficient. Here we showed how the system of equations can be solved numerically by the matrix-continued-fraction (MCF) techniques.

Although the MCF method permitted the efficient numerical solution over a wide range of values of friction coefficient and temperature, the procedure is limited in the low-temperature case that turns out to be of special interest. For this reason, we resorted to long stochastic simulations of the Langevin equations in order to explore the asymptotic behavior of the diffusion coefficient in the limit of weak noise. Our results illustrate that, contrary to speculations in the literature, the diffusion coefficient of underdamped Brownian particles is enhanced in a finite range of forces that is well within the region of bistability of the deterministic velocity dynamics. We could support these findings and explain them in greater detail by means of a two-state theory for the velocity, in which switching rates depend in a specific way on the temperature. One consequence of this theory is that for certain values of the bias force the diffusion coefficient passes through a maximum as a function of temperature. These results underpin the importance of a thorough theoretical exploration of the transition rates between locked and running states in and close to the parameter region of giant enhancement of diffusion.

Summarizing, we have unveiled asymptotic weak-noise properties of a simple but important model of statistical physics. We hope that our investigation may trigger experimental work aiming at verifications of the finite range of forces and the maximized diffusion vs temperature.

APPENDIX: SOLUTION OF THE DIFFUSION COEFFICIENT IN TERMS OF MATRIX-CONTINUED FRACTIONS

Here we show how to apply the matrix-continued-fraction techniques to the problem of solving the partial differential equations Eq. (22) and Eq. (23) and to obtain the velocity and diffusion coefficient. We start with the problem of solving for the stationary density and the mean velocity, a task that has been achieved already by Risken *et al.* and is also presented in some detail in his textbook [1] (chapters 9 and 11). We nevertheless include this calculation here in order to make the presentation self-contained and to introduce the basic idea of the method and the notation.

We expand the desired functions in a set of eigenfunctions chosen appropriately according to the boundary conditions: harmonic functions with respect to x and Hermite functions with respect to the velocity. We start with the stationary density $p(x,v)$ and then repeat the derivation for $g(x,v)$.

1. Determination of the coefficients for the stationary solution

Following Ref. [1] we make the ansatz

$$p(x,v) = \phi_0(v) \sum_{p=0}^{\infty} \sum_{m=-\infty}^{+\infty} c_p^m e^{imx} \phi_p(v), \tag{A1}$$

where ϕ_p are the Hermite functions obeying

$$y\phi_p = \frac{\alpha}{\sqrt{2}}(\sqrt{p+1}\phi_{p+1} + \sqrt{p}\phi_{p-1}), \tag{A2}$$

$$(\phi_0\phi_p)' = -\frac{1}{\alpha}\sqrt{2(p+1)}\phi_0\phi_{p+1}, \tag{A3}$$

$$\int dy \phi_p \phi_q = \delta_{pq}. \tag{A4}$$

with a still undetermined scale factor α.

If we insert Eq. (A1) into the steady state FPE, Eq. (22) and apply Eq. (A2) and Eq. (A3), we obtain

$$\begin{aligned}\sum\sum c_p^m \Big\{ & -ime^{imx}\frac{\alpha}{\sqrt{2}}(\sqrt{p+1}\phi_{p+1} + \sqrt{p}\phi_{p-1}) \\ & - \gamma e^{imx}(\sqrt{(p+1)(p+2)}\phi_{p+2} + p\phi_p) \\ & + \gamma kT e^{imx}\frac{2\sqrt{(p+1)(p+2)}}{\alpha^2}\phi_0\phi_{p+2} \\ & + \frac{F}{\alpha}\sqrt{2(p+1)}e^{imx}\phi_0\phi_{p+1} \\ & + \frac{id}{2}\frac{\sqrt{2(p+1)}}{\alpha}\phi_0\phi_{p+1}(e^{i(m+1)x} - e^{+i(m-1)x})\Big\} = 0,\end{aligned} \tag{A5}$$

where we have used that $U_0'(x) = d\sin x = d(e^{ix} - e^{-ix})/(2i)$. If we choose the free parameter α in Eq. (A2) and Eq. (A3) as

$$\alpha = \sqrt{2kT}, \tag{A6}$$

the third line in Eq. (A5) cancels with the first term of the second line (i.e., all terms vanish that involve ϕ_{p+2}).

Applying the operator $\frac{1}{2\pi}\int_0^{2\pi} dx e^{-inx} \int_{-\infty}^{+\infty} dv \phi_q/\phi_0$ to the left-hand side yields:

$$\begin{aligned}\sum_p \sum_m c_p^m \Big\{ & -in\delta_{m,n}\sqrt{kT}(\sqrt{p+1}\delta_{q,p+1} + \sqrt{p}\delta_{q,p-1}) \\ & - \gamma\delta_{m,n}p\delta_{q,p} + \frac{F}{\sqrt{kT}}\sqrt{p+1}\delta_{m,n}\delta_{q,p+1} \\ & + \frac{id}{2}\sqrt{\frac{p+1}{kT}}\delta_{q,p+1}(\delta_{n,m+1} - \delta_{n,m-1})\Big\} = 0.\end{aligned} \tag{A7}$$

Because for a given q only three different values of p contribute, this can be expressed by the following single sum

over m:

$$\sum_m c_{q-1}^m \sqrt{\frac{q}{kT}}\left[(F - inkT)\delta_{m,n} + \frac{id}{2}(\delta_{n,m+1} - \delta_{n,m-1})\right] - \sum_m c_q^m q\gamma\delta_{m,n} - \sum_m c_{q+1}^m \sqrt{kT(q+1)}in\delta_{mn} = 0, \quad \text{(A8)}$$

which in turn can be regarded as one row of a matrix multiplication with a vector

$$\sqrt{q}\hat{D}\cdot\vec{c}_{q-1} + \gamma q\cdot I\cdot\vec{c}_q + \sqrt{q+1}\bar{D}\vec{c}_{q+1} = 0, \quad \text{(A9)}$$

a vector recurrence relation between $\vec{c}_{q-1}$,$\vec{c}_q$, and $\vec{c}_{q+1}$, where $\vec{c}_q$ is defined as

$$\vec{c}_q = \begin{pmatrix} \cdots \\ c_q^{m-1} \\ c_q^m \\ c_q^{m+1} \\ \cdots \end{pmatrix}. \quad \text{(A10)}$$

The entries of the matrices $\hat{D}$ and $\bar{D}$ are given by

$$(\hat{D})_{m,n} = \frac{\delta_{m,n}(inkT - F) - id(\delta_{n,m+1} - \delta_{n,m-1})/2}{\sqrt{kT}} \quad \text{(A11)}$$

$$(\bar{D})_{m,n} = in\sqrt{kT}\delta_{m,n}. \quad \text{(A12)}$$

The tridiagonal vector recurrence relation is solved as follows: we first introduce a (still unknown) matrix S_q defined by

$$\vec{c}_{q+1} = S_q\vec{c}_q. \quad \text{(A13)}$$

Because the normalization condition and the structure of the Fokker-Planck equation determine some of the vector entries in $\vec{c}_0$ and $\vec{c}_1$ (see below), the knowledge of the matrices $S_0, \ldots S_q$ will give us knowledge about all the expansion coefficients up to order q. Inserting Eq. (A13) into the recurrence relation, yields:

$$\sqrt{q}\hat{D}\vec{c}_{q-1} + \gamma q\cdot IS_{q-1}\vec{c}_{q-1} + \sqrt{q+1}\bar{D}S_qS_{q-1}\vec{c}_{q-1} = 0, \quad \text{(A14)}$$

where I is the identity matrix. We can also write

$$[\sqrt{q}\hat{D} + (\gamma q\cdot I + \sqrt{q+1}\bar{D}S_q)S_{q-1}]\vec{c}_{q-1} = 0. \quad \text{(A15)}$$

This relation is certainly satisfied, if the square bracket vanishes, which leads to

$$S_{q-1} = -\sqrt{q}(\gamma q\cdot I + \sqrt{q+1}\bar{D}S_q)^{-1}\cdot\hat{D}. \quad \text{(A16)}$$

Note that $(\ldots)^{-1}$ indicates a matrix inversion, i.e., a fraction of matrices.

To simplify the numerics it is convenient to use rescaled matrices [see Ref. [1], Eq. (11.172)]

$$A_q = -\gamma\sqrt{q+1}S_q, \quad \text{in particular } S_0 = -\frac{1}{\gamma}A_0 \quad \text{(A17)}$$

in terms of which the above matrix fraction reads

$$A_{q-1} = \frac{1}{I - (q\gamma^2)^{-1}\bar{D}A_q}\hat{D} \quad \text{(A18)}$$

$$= (I - (q\gamma^2)^{-1}\bar{D}A_q)^{-1}\hat{D}, \quad \text{(A19)}$$

where in the notation of the second line the order of matrix multiplications becomes more transparent. Repeated application of this relation yields the matrix continued fraction

$$A_{q-1} = \cfrac{1}{I - \frac{1}{q\gamma^2}\bar{D}\cfrac{1}{I - \frac{1}{(q+1)\gamma^2}\bar{D}\cfrac{1}{I - \frac{1}{(q+2)\gamma^2}\bar{D}\frac{1}{\cdots}\hat{D}}\hat{D}}\hat{D}}\hat{D} = \left[I - \frac{1}{q\gamma^2}\bar{D}\left(I - \frac{1}{(q+1)\gamma^2}\bar{D}\ldots\hat{D}\right)^{-1}\hat{D}\right]^{-1}\hat{D}, \quad \text{(A20)}$$

which can be continued on the right-hand side to A_Q where Q is sufficiently high. If we set A_{Q+1} to zero, then $A_Q = \hat{D}$ and we can calculate all A_q from $q = 0$ to $q = Q - 1$ by the above recursive relation. Clearly, Q will be one of the parameters of the numerical procedure of which our final result should not depend. In practice, we have to repeat the above procedure for different values of Q until the final statistics does not change anymore by increasing Q within a desired accuracy.

The procedure above requires the inversion of complex-valued matrices. The dimension of these matrices depend on the number $2M + 1$ of eigenfunctions $\exp[imx]$ ($m = -M, \ldots, M$) that we need with respect to the spatial variable. Lower noise results usually in a more strongly peaked distribution and will thus require a larger number M and thus larger matrices, which in turn are more difficult to invert. This implies that although modern computers can store and invert rather large matrices, the procedure has its limitations exactly in the weak-noise limit.

Once we have computed all the matrices A_q and S_n, we obtain the coefficients contained in the vectors $\vec{c}_n$ by using the following additional information. First, the normalization of the density implies

$$1 = \int_0^{2\pi} dx \int_{-\infty}^{+\infty} dv \sum_p^m c_p^m e^{imx}\phi_0(v)\phi_p(v) = 2\pi c_0^0 \quad \text{(A21)}$$

and thus

$$c_0^0 = \frac{1}{2\pi}. \quad \text{(A22)}$$

Second, we can consider Eq. (A9) for $q = 0$, keeping in mind that $c_{-1}^m = 0\ \forall m$ and that the term proportional to q does not enter, the simple structure of the matrix $\bar{D}$, which has only entries on the diagonal, leads to

$$c_1^m = 0 \ \ \forall m \neq 0. \quad \text{(A23)}$$

Hence, we know one component of the vector $\vec{c}_0$ and $2M$ components of the vector $\vec{c}_1$ and have to combine this knowledge to determine all components of $\vec{c}_0$, $\vec{c}_1$ and then the remaining vectors $\vec{c}_q$ with $q \geqslant 2$.

We know that $\vec{c}_1 = S_0\vec{c}_0$ or

$$\vec{c}_0 = H\vec{c}_1, \quad \text{where } H = S_0^{-1}. \quad \text{(A24)}$$

In particular,

$$c_0^0 = \frac{1}{2\pi} = \sum_m H_{0,m} c_1^m = H_{0,0} c_1^0 \quad \Rightarrow \quad c_1^0 = \frac{1}{2\pi H_{0,0}}. \tag{A25}$$

The coefficient c_1^0 is important because it determines uniquely the mean velocity:

$$\begin{aligned}\langle v\rangle &= \int_0^{2\pi} dx \int_{-\infty}^{\infty} dv\ v\ p(x,v) \\ &= \int_0^{2\pi} dx \int_{-\infty}^{\infty} dv \sum_{p,m} c_p^m e^{imx} \phi_0 \sqrt{kT} \\ &\quad \times (\sqrt{p+1}\phi_{p+1} + \sqrt{p}\phi_{p-1}) \\ &= 2\pi\sqrt{kT} c_1^0 = \frac{\sqrt{kT}}{H_{0,0}}.\end{aligned} \tag{A26}$$

The remaining c_0^m are determined by

$$c_0^m = \sum_n H_{m,n} c_1^n = \sum_n H_{m,n} c_1^0 \delta_{n,0} = H_{m,0} c_1^0 = \frac{1}{2\pi} \frac{H_{m,0}}{H_{0,0}} \tag{A27}$$

and the marginal density is given by

$$p(x) = \int dv\ p(x,v) = \frac{1}{2\pi} \sum_{m=-M}^{M} \frac{H_{m,0}}{H_{0,0}} e^{imx}. \tag{A28}$$

The higher vectors are obtained by up iteration

$$\vec{c}_2 = S_1 \cdot \vec{c}_1, \quad c_2^m = \sum (S_1)_{m,n} c_1^0 \delta_{n,0} = (S_1)_{m,0}, \tag{A29}$$

$$\vec{c}_{p+1} = S_p \cdot \vec{c}_p = -\frac{1}{\gamma\sqrt{p+1}} A_p \vec{c}_p, \quad p \geqslant 2. \tag{A30}$$

2. Solving for the function $g(x,y)$ and the diffusion coefficient

We expand the function $g(x,v)$, which determines the diffusion coefficient, in terms of Hermite and harmonic functions

$$g(x,v) = \sum_p \sum_m h_p^m e^{imx} \phi_0 \phi_p. \tag{A31}$$

As in the expansion of $p(x,v)$, certain coefficients are already set by the defining equations of $g(x,v)$. First, inserting the expansion into Eq. (20) yields

$$h_0^0 = 0. \tag{A32}$$

Second, according to Eq. (25), the diffusion coefficient is given by just one of the coefficients

$$D_{\text{eff}} = \int_0^{2\pi} dx \int_{-\infty}^{\infty} dv\ v\ g(x,v) = 2\pi\sqrt{kT} h_1^0. \tag{A33}$$

Another set of coefficients arises from the recurrence relation in a special case (see below). Next, we insert the expansions for $p(x,v)$ and $g(x,v)$ into Eq. (23) and apply the operator $\frac{1}{2\pi}\int_0^{2\pi} dx e^{-inx} \int_{-\infty}^{+\infty} dv \phi_q/\phi_0$. On the left-hand side, we obtain the same terms as in the equation for $p(x,v)$, only that the coefficients c_q^n are replaced by h_q^n. On the right-hand side, the expansion of $p(x,v)$ yields

$$\begin{aligned}&\frac{1}{2\pi}\int_0^{2\pi} dx e^{-inx} \int_{-\infty}^{\infty} dv \frac{\phi_q}{\phi_0}(\langle v\rangle - v) \sum\sum c_p^m e^{imx} \phi_0 \phi_p \\ &= \sum_m \langle v\rangle \delta_{nm} c_q^m - \delta_{n,m}\sqrt{kT}(\sqrt{q+1} c_{q+1}^m + \sqrt{q} c_{q-1}^m) \\ &= a_q^n,\end{aligned} \tag{A34}$$

defining the entries of an inhomogeneity vector $\vec{a}_q$. The inhomogeneous recurrence relation can be written as

$$-\sqrt{q}\hat{D}\vec{h}_{q-1} - \gamma q I \vec{h}_q - \sqrt{q+1}\bar{D}\vec{h}_{q+1} = \vec{a}_q. \tag{A35}$$

Specifically for $q = 0$, this relation reads

$$-\bar{D}\vec{h}_1 = \langle v\rangle \vec{c}_0 - \sqrt{kT}\vec{c}_1 \tag{A36}$$

and because of the diagonal structure of the matrix $\bar{D}$ [cf. Eq. (A12)] it follows that

$$h_1^m = i\frac{\langle v\rangle}{m\sqrt{kT}} c_0^m \quad \forall m \neq 0. \tag{A37}$$

Together with $h_0^0 = 0$ from Eq. (A32) and similarly to the situation in the previous subsection, we thus know $2M+1$ coefficients.

To solve the inhomogeneous relation Eq. (A35), we follow Risken [see p. 213, Eq. (9.82)] and make the ansatz

$$\vec{h}_{q+1} = S_q \vec{h}_q + \vec{b}_{q+1}, \tag{A38}$$

where $\vec{b}_{q+1}$ is yet to be determined. Inserting this into Eq. (A35) (all nonzero terms brought to one side)

$$\begin{aligned}0 &= \sqrt{q}\hat{D}\vec{h}_{q-1} + \gamma q I \vec{h}_q + \sqrt{q+1}\bar{D}\vec{h}_{q+1} + \vec{a}_q \\ &= \sqrt{q}\hat{D}\vec{h}_{q-1} + (\gamma q I + \sqrt{q+1}\bar{D}S_q)(S_{q-1}\vec{h}_{q-1} + b_q) \\ &\quad + \sqrt{q+1}\bar{D}b_{q+1} + \vec{a}_q \\ &= [-\sqrt{q}\hat{D} - (\gamma q I + \sqrt{q+1}\bar{D}S_q)S_{q-1}]\vec{h}_{q-1} \\ &\quad \underline{-(\gamma q I + \sqrt{q+1}\bar{D}S_q)b_q - \sqrt{q+1}\bar{D}b_{q+1} - \vec{a}_q.}\end{aligned} \tag{A39}$$

The last equation is satisfied if both the square bracket as well as the underlined terms vanish separately. The square bracket set to zero is exactly Eq. (A15), i.e., the same equation we had found previously for the matrices S_q and hence also the solution in terms of the matrix-continued fraction will satisfy this equation. Vanishing of the underlined terms implies

$$\vec{b}_q = -(\gamma q I + \sqrt{q+1}\bar{D}S_q)^{-1}(\vec{a}_q + \sqrt{q+1}\bar{D}\vec{b}_{q+1}). \tag{A40}$$

Suppose we know all the matrices S_q [which we previously had to determine in order to find the stationary density $p(x,v)$] and we start at a sufficiently large value $q = Q$, we set $\vec{b}_{Q+1}$ to zero and obtain

$$b_Q = -(\gamma Q \cdot I + \sqrt{Q+1}\bar{D}S_Q)^{-1}\vec{a}_Q. \tag{A41}$$

We can then iterate Eq. (A40) down to $\vec{b}_1$. Then

$$\vec{h}_1 = S_0\vec{h}_0 + \vec{b}_1 \quad \Rightarrow \quad \vec{h}_0 = S_0^{-1}(\vec{h}_1 - \vec{b}_1) = H(\vec{h}_1 - \vec{b}_1), \tag{A42}$$

where we used the matrix H defined in the previous subsection. Using our knowledge about h_0^0 leads to

$$\begin{aligned} 0 = h_0^0 &= \sum_m H_{0,m}\left(h_1^m - b_1^m\right), \\ &= H_{0,0}\left(h_1^0 - b_1^0\right) + \sum_{m\neq 0} H_{0,m}\left(h_1^m - b_1^m\right). \end{aligned} \tag{A43}$$

From this relation we obtain

$$h_1^0 = b_1^0 - \sum_{m\neq 0} \frac{H_{0,m}}{H_{0,0}}\left(h_1^m - b_1^m\right) \tag{A44}$$

$$= -i \sum_{m\neq 0} \frac{H_{0,m}}{H_{0,0}} \frac{\langle v\rangle}{m\sqrt{kT}} c_0^m + \sum_m \frac{H_{0,m} b_1^m}{H_{0,0}}, \tag{A45}$$

where we have used Eq. (A37). This then determines the diffusion coefficient according to Eq. (A33)

$$D_{\text{eff}} = \frac{2\pi}{H_{0,0}} \left(\sqrt{kT} \sum_m H_{0,m} b_1^m - i \frac{\langle v\rangle}{m} \sum_{m\neq 0} H_{0,m} c_0^m \right). \tag{A46}$$

[1] H. Risken, *The Fokker-Planck Equation* (Springer, Berlin, 1984).

[2] L. Longobardi, D. Massarotti, G. Rotoli, D. Stornaiuolo, G. Papari, A. Kawakami, G. P. Pepe, A. Barone, and F. Tafuri, Phys. Rev. B **84**, 184504 (2011).

[3] P. Fulde, L. Pietronero, W. R. Schneider, and S. Strässler, Phys. Rev. Lett. **35**, 1776 (1975).

[4] R. L. Stratonovich, *Topics in the Theory of Random Noise* (Gordon and Breach, New York, 1967).

[5] H. Vollmer and H. Risken, J. Phys. B. Cond. Mat. **52**, 259 (1983).

[6] P. Jung and H. Risken, Z. Phys. B. Cond. Mat. **54**, 357 (1984).

[7] P. Jung and B. J. Berne, in *New Trends in Kramers Reaction Rate Theory: Understanding Chemical Reactivity*, edited by P. Talkner and P. Hänggi (Kluwer Academic Publishers, Dordrecht, 1995), p. 67.

[8] G. Costantini and F. Marchesoni, Europhys. Lett. **48**, 491 (1999).

[9] P. Reimann, C. Van den Broeck, H. Linke, P. Hänggi, J. M. Rubi, and A. Pérez-Madrid, Phys. Rev. Lett. **87**, 010602 (2001).

[10] B. Lindner, M. Kostur, and L. Schimansky-Geier, Fluct. Noise Lett. **1**, R25 (2001).

[11] K. Lindenberg, A. M. Lacasta, J. M. Sancho, and A. H. Romero, New J. Phys. **7**, 29 (2005).

[12] K. Lindenberg, J. M. Sancho, A. M. Lacasta, and I. M. Sokolov, Phys. Rev. Lett. **98**, 020602 (2007).

[13] J. M. Sancho and A. M. Lacasta, Eur. Phys. J.-Spec. Top. **187**, 49 (2010).

[14] I. G. Marchenko and I. I. Marchenko, Europhys. Lett. **100**, 50005 (2012).

[15] I. Marchenko, I. Marchenko, and A. Zhiglo, Eur. Phys. J. B **87**, 10 (2014).

[16] S.-H. Lee and D. G. Grier, Phys. Rev. Lett. **96**, 190601 (2006).

[17] M. Evstigneev, O. Zvyagolskaya, S. Bleil, R. Eichhorn, C. Bechinger, and P. Reimann, Phys. Rev. E **77**, 041107 (2008).

[18] S. Albaladejo, M. I. Marqués, F. Scheffold, and J. J. Sáenz, Nano Lett. **9**, 3527 (2009).

[19] R. Hayashi, K. Sasaki, S. Nakamura, S. Kudo, Y. Inoue, H. Noji, and K. Hayashi, Phys. Rev. Lett. **114**, 248101 (2015).

[20] B. Lindner, New J. Phys. **9**, 136 (2007).

[21] B. Lindner and E. M. Nicola, Phys. Rev. Lett. **101**, 190603 (2008).

[22] P. Reimann, Phys. Rep. **361**, 57 (2002).

[23] C. Van den Broeck, Physica A **168**, 677 (1990).

[24] E. Ben-Jacob, D. J. Bergman, B. J. Matkowsky, and Z. Schuss, Phys. Rev. A **26**, 2805 (1982).

[25] M. Büttiker, E. P. Harris, and R. Landauer, Phys. Rev. B **28**, 1268 (1983).

[26] R. Cristiano and P. Silvestrini, J. Appl. Phys. **59**, 1401 (1986).